Numerical simulations of eddies in the Gulf of Lion

Z. Y. Hu [a,*] A. M. Doglioli [a], A. A. Petrenko [a], P. Marsaleix [b], I. Dekeyser [a],

[a] *Aix-Marseille Université, CNRS, Laboratoire d'Océanographie Physique et Biogéochimique, UMR 6535, OSU/Centre d'Océanologie de Marseille, France*

[b] *Université Paul Sabatier, CNRS, Laboratoire d'Aérologie, Toulouse, France*

Abstract

We present realistic simulations of mesoscale anticyclonic eddies, present in the western side of the Gulf of Lion and generally observed in satellite imagery during July and August. A nested model of 1-km resolution covering the Gulf of Lion is implemented from a coarse model of 3-km resolution. The models use an upwind-type advection-diffusion scheme, in which the numerical diffusion term is adjusted by an attenuation coefficient. Sensitivity tests have been carried out, varying the model spatial resolution and the attenuation coefficient to reproduce the (sub)mesoscale structures. A wavelet technique is applied to analyze the modelled horizontal relative vorticity in order to define the area, position and tracking duration of the eddy structures. Comparisons between the modelled eddies and those observed by satellite have allowed us to choose the best model setup. With this setup, the studied anticyclonic eddy lasted for 60 days.

Key words: Numerical modeling; (sub)mesoscale eddies; northwestern Mediterranean Sea;

1 Introduction

The Gulf of Lion (hereafter GoL), is located in the northwestern Mediterranean Sea (Fig. 2). This large continental shelf has approximatively the shape of a semi-circle with a 100 km radius. Its continental slope is cut by numerous canyons. Three main forcings of the shelf circulation are: i) the strong northerly

* Corresponding author.
Email address: ziyuan.hu@univmed.fr (Z. Y. Hu).

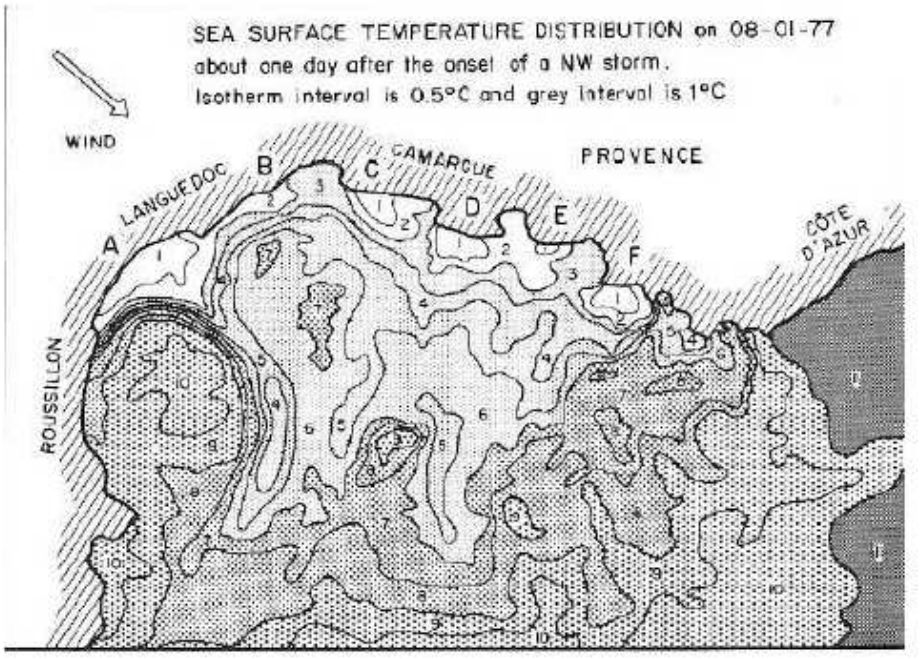

Fig. 1. Infrared thermography on the August 1, 1977 at about 09 00 TU. (From Millot, 1982)

and northwesterly continental winds (the Mistral and the Tramontane); ii) the Northern Current (hereafter NC) which represents the northern branch of the cyclonic circulation of the western Mediterranean basin and flows along the continental slope from the Ligurian Sea to the Catalan Sea (Millot, 1990); iii) the Rhône River which is the main fresh water source of the GoL. A general description of the hydrodynamics of the GoL is provided by Millot (1990). He was the pioneer in describing an anticyclonic circulation in the western part of the gulf following upwelling phenomena and an offshore drift of surface water (Fig. 1) (Millot, 1979, 1982). In both data and model, Estournel et al. (2003) showed an anticyclonic eddy located at the center of the GoL continental shelf or an anticyclonic circulation covering the western and center parts of the GoL. The eddy-like structures in the western part of the GoL, potentially influenced by the distal plume extension of the Rhône river, could play an important role in the shelf-offshore transport of nutrients and phytoplankton because of the presence of the NC nearby. However, to our knowledge, no one has yet studied and modelled the dynamics of the eddy structures in this area. Hence, the LAgrangian Transport EXperiment (LATEX) projet (2008-2011) has been initiated in order to study the role of (sub)mesoscale (5-25 km) structures on shelf-offshore exchanges in this area. The LATEX strategy combines use of data from an inert tracer release (SF_6), Lagrangian drifters, satellites and Eulerian moorings with numerical modelling. In this framework, starting from regional numerical model (Estournel et al., 2007; Bouffard et al., 2008), we implemented a nested high-resolution shelf-scale model to reproduce accurately the processes on the shelf at the (sub)mesoscale. We paid special attention to two aspects of the model: the spatial grid resolution and the diffusion numerical scheme. The latter is known to play a key role because it controls the dissipation of the model energy and prevents the generation of

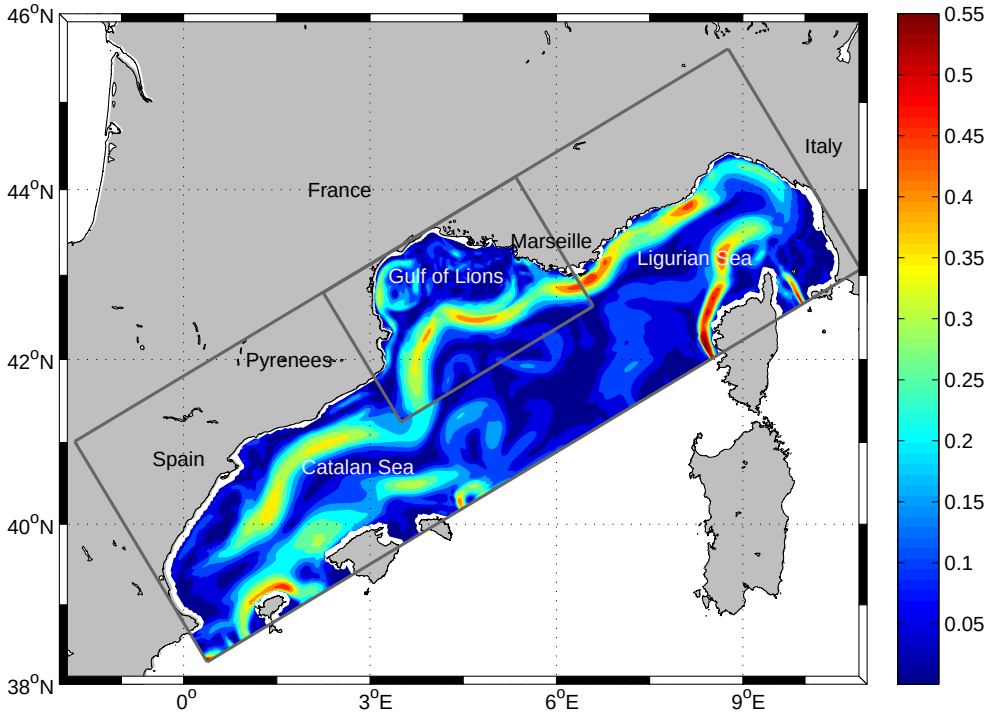

Fig. 2. Model domains. The larger (smaller) rectangle represents the model domain of the 3-km (1-km) resolution. Shaded color represents the intensity of the modelled horizontal current [m s^{-1}] at 20-m depth on July 25, 2001.

numerical instabilities.

In this paper we present the first results of a sensitivity study that allow us to find the best model setup to reproduce anticyclonic eddies in the western side of the GoL. Our numerical results are validated by a qualitative comparison with satellite imagery.

2 Methods

Symphonie, the model used for the present study, is a 3-D primitive equation, free surface, sigma coordinate ocean model, based on Boussinesq and hydrostatic approximations. Components of current, temperature and salinity are computed on an Arakawa-C grid using a classic finite difference method detailed in Marsaleix et al. (2006, 2008). The vertical turbulence closure is achieved through a prognostic equation for the turbulent kinetic energy and a diagnostic equation for the mixing and dissipation length scales (Gaspar et al., 1990). During the last ten years, the Symphonie has been used widely and successfully by the coastal ocean modeling community. The realistic simulations of this model have contributed to the study of: i) the wind-induced circulations in the GoL (Auclair et al., 2003; Estournel et al., 2003; Petrenko et al., 2005, 2008); ii) the intrusion of the NC onto the continental shelf (Auclair et al.,

2001; Gatti, 2008); iii) dense-water formation and cascading phenomena over the continental shelf (Dufau-Julliand et al., 2004; Herrmann and Somot, 2008; Herrmann et al., 2008; Ulses et al., 2008a,b) and iv) the Rhône river plume circulation (Marsaleix, 1998; Estournel, 2001).

For this work, a coarse model extends throughout the northern part of the western basin of the Mediterranean Sea with a horizontal resolution of 3 km, while a nested model focuses on the GoL with a horizontal resolution of 1 km (Fig. 2). These values respect the grid ratio proposed by Spall and Holland (1991) and are smaller than the Rossby radius of this area (15 km suggested by Grilli and Pinardi (1998)). A one-way nesting, described in (Ulses et al., 2005), is adopted. Realistic simulations are run over the whole 2001 year, which is of special interest since both satellite data used in this paper (Fig. 3a) and cruise data (not shown in this paper) are available. Data from the weather-forecast model Aladin with a high spatial (0.1° x 0.1°) and temporal (3h) resolution are used as meteorological forcings. The air-sea fluxes are estimated thanks to bulk formulae (Estournel et al., 2007). The large scale field from a general circulation model of the mediterranean sea (OGCM) is applied as an inital state of the presented simulations and is used to force the Symphonie model. Daily fluxes of fresh water supplied by the major rivers (Rhône, Hérault, Aude and Orb) constitute the river input (data from the *Compagnie Nationale du Rhône* and the *Directions Départementales de l'Équipement*).

In the following, a short description of the advection-diffusion scheme is given to introduce the reader to the meaning of our sensitivity study. Momentum equations use an upwind advection scheme. As shown by James (1996), the standard upwind scheme can be written as the combination of a centered advection scheme and a Laplacian type dissipation term, in which the viscosity coefficient is given by:

$$A = |u|\frac{\Delta x}{2} \tag{1}$$

where u and Δx are respectively the current component and the grid mesh size related to the Ox axis.

Combined with a Leapfrog time-stepping technique, the advection-diffusion scheme becomes:

$$\begin{aligned}\frac{{\phi_i}^{t+\Delta t} - {\phi_i}^{t-\Delta t}}{2\Delta t} = &- \frac{{u^t}_{i+1/2}}{\Delta x}\frac{\phi_i^t + \phi_{i+1}^t}{2} + \frac{{u^t}_{i-1/2}}{\Delta x}\frac{\phi_i^t + \phi_{i-1}^t}{2} \\ &+ \frac{A_{i+1/2}}{\Delta x}\frac{\phi_{i+1}^{t-\Delta t} - \phi_i^{t-\Delta t}}{\Delta x} - \frac{A_{i-1/2}}{\Delta x}\frac{\phi_i^{t-\Delta t} - \phi_{i-1}^{t-\Delta t}}{\Delta x}\end{aligned} \tag{2}$$

where ϕ is any of the two horizontal current components, Δt the model time

step and i the horizontal Ox grid index (for the sake of clarity, discretization related to the Oy and Oz grid axes is intentionally omitted). The first two terms of the right hand of Eq.(2) correspond to advection processes and the last two terms to diffusion processes. In the diffusion terms, we use the values obtained at the previous time step $(t - \Delta t)$ for numerical stability reasons, while, in the advection terms, we use the current time step (t) for energy conservation reasons (Marsaleix et al., 2008). The value of the horizontal viscosity coefficient provided by Eq.(1) can be quite large. With the size of the coarse horizontal mesh (3 km), a current of only 0.01 ms^{-1} induces a viscosity coefficient of 15 m^2s^{-1}. In a realistic context with much stronger currents, the energy dissipation using an upwind advection scheme probably becomes excessive. However, the opportunity to prevent the development of numerical instabilities through an increase of energy dissipation is rather attractive and pleads for an upwind-type advection-diffusion scheme. A compromise can be found in using an attenuated value of Eq.(1), namely:

$$\tilde{A} = \delta \cdot |u| \frac{\Delta x}{2} \tag{3}$$

The value of the non-dimensional coefficient δ varies between 0 and 1. When $\delta = 0$, the dissipative effect is cancelled; when $\delta = 1$, the dissipation is totally taken into account.

Table 1 summarizes the numerical experiments. *exp0*, *exp1* and *exp2* represent the simulations of the northern part of the western basin of the Mediterranean Sea with 3-km resolution. *exp3* and *exp4* are the nested simulations of GoL with 1-km resolution. In the first experiment(*exp0*), the horizontal viscosity coefficient has been fixed equal to 15 m^2s^{-1} following Dufau-Julliand et al. (2004) and Estournel et al. (2007). Then, we performed two experiments in which, for a fixed resolution of 3 km, we varied the δ value: 0.2 in *exp1* and 0.8 in *exp2*. Analogously, we performed two experiments for a fixed resolution of 1 km with $\delta = 0.2$ in *exp3* and $\delta = 0.8$ in *exp4*. For the sake of simplicity, in *exp3* and *exp4*, the two nested models are forced by the same coarse model: *exp1*.

Then, to objectively analyze all simulation results, we use wavelet analysis, which is a useful and powerful tool. Indeed, wavelets have been applied, for the ocean, to the numerical resolution of Kelvin and Rossy waves (Jameson and Miyama, 2000) and to time-evolving structures such as eddies and fronts described by numerical modeling or by satellite data (Luo and Jameson, 2002). In this work we applied the method developed by Doglioli et al. (2007), based on wavelet analysis of horizontal slices of modelled relative vorticity, to identify and to track the localized structures. First, the wavelet technique extracts eddy structures from model gridcells. The area of identified structure is calculated as the sum of gridcell areas. The center of eddies is defined as the gridpoint

experiment code	resolution [km]	δ [non-dimensional]	eddy area mean ± std [km^2]	tracking duration [days]
exp0	3	* $\tilde{A} = 15$ [m^{2}s^{-1}]	1035 ± 407	42
exp1	3	0.2	950 ± 398	33
exp2	3	0.8	1853 ± 1753	45
exp3	1	0.2	694 ± 446	70
exp4	1	0.8	1193 ± 543	56

Table 1
Summary of numerical experiment setups and results.
* N.B: here, the horizontal viscosity coefficient is taken as a fixed value and, hence, does not contain the attenuation coefficient δ.

of local maximum in absolute relative vorticity over the eddy area. Then, for an eddy identified at a specific time (*t*), time tracking can be performed both backward (*t-1*) and forward (*t+1*) in time until a certain criterion cannot be satisfied, which stops the analysis. The reader is referred to Doglioli et al. (2007) for more details. The 'birth' and 'death' of the eddy correspond to the last instant of the backward and forward tracking respectively. The eddy life is computed in this way and a time series of eddy area is obtained to provide useful information on the evolution of the shape of the eddy. In this present work, analysis is performed at 20-m depth because it is the operational depth (SF_6 release and Lagrangian drifters anchoring) chosen for the future LATEX cruises scheduled to take place in September. Indeed, this depth generally corresponds to half the depth of the mixed layer at that period. The eddy area at 20-m is averaged and the corresponding standard deviation is calculated over the tracking duration (Table 1). The latter is not only used as a mean error but also provides insight on the variability of the eddy.

3 Results and Discussion

Figure 1 shows imbricated horizontal slices of the modelled current intensity on July 25, 2001 at 20-m depth for *exp1* (3 km) over the large domain minus the GoL and *exp4* (1 km), in the GoL. The continuation of the NC at the northeastern and southwestern boundary edges of the nested model shows that the nesting works very well. The major features in the GoL such as the NC, eddies and filaments are reproduced very well. Indeed, the NC's width, depth, velocity and meanders with its seasonal variations (not shown here) are comparable to previous measurements (Millot, 1990; Conan and Millot, 1995; Albérola and Millot, 2003; Petrenko, 2003; Petrenko et al., 2005). In

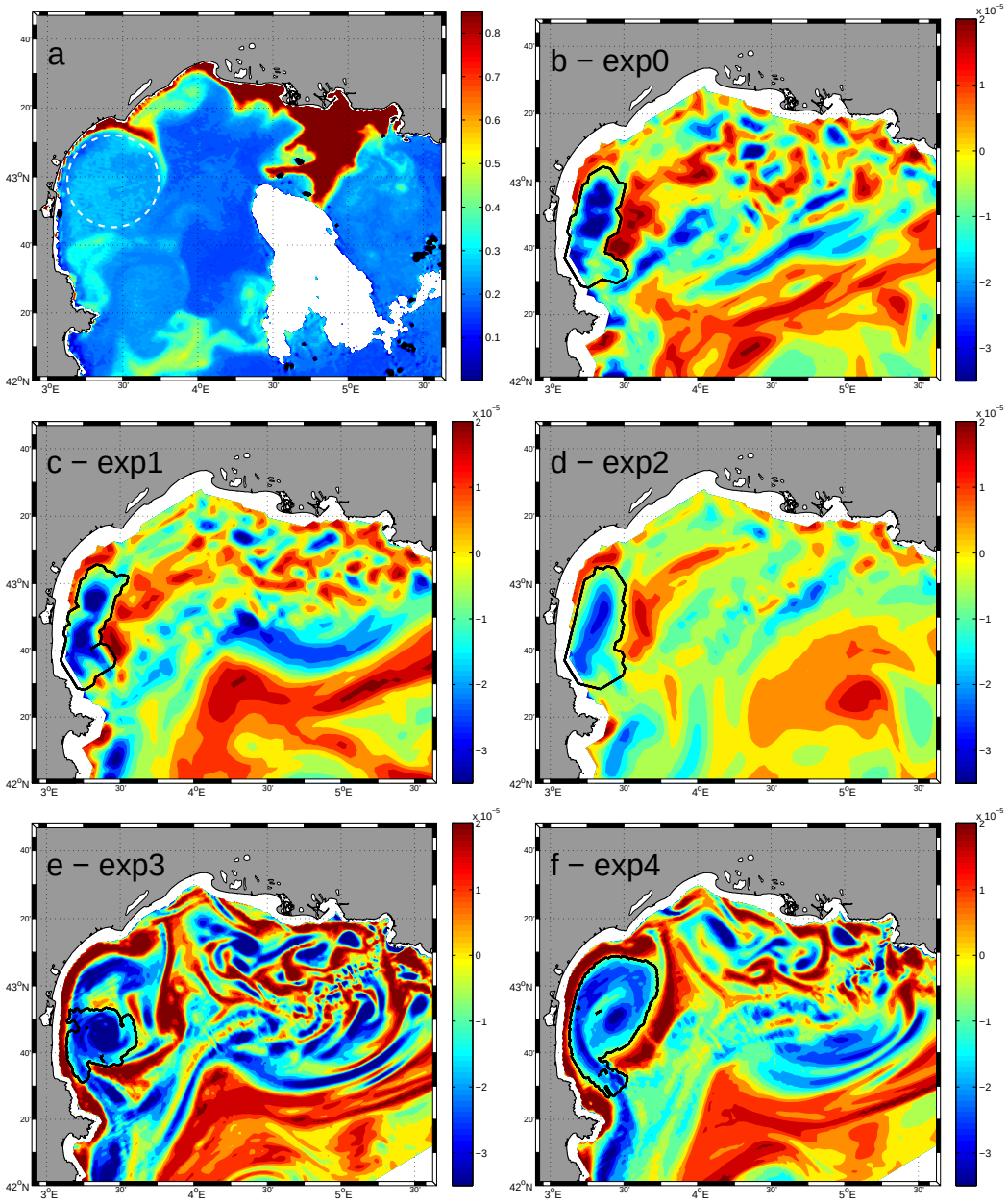

Fig. 3. Comparison of the signature of the anticyclonic eddy on a chlorophyll *a* [mg m^{-3}] map and the eddy, as identified by the wavelet analysis (contour black) of simulated relative vorticity [s^{-1}] on July 25, 2001. a) SeaWiFs image processed with OC4 (courtesy E.Bosc); the dashed white circle represents the eddy area. Relative vorticity at 20-m depth from simulations b) *exp0*, c) *exp1*, d) *exp2*, e) *exp3* and f) *exp4*. See text for more explanations.

the relative vorticity field, anticyclonic (cyclonic) features appear in the NC's internal (external) edge (Fig. 3b-f). Among all the (sub)mesoscale structures reproduced in the model, special attention is given here to an intense anticyclonic eddy frequently observed in the western side of the GoL. This anticyclonic eddy is clearly observed in the chlorophyll *a* concentrations derived from

satellite data (Fig. 3a). Moreover, this structure corresponds well, in position and size, to the one observed at the same period of the year in SST satellite images by Millot (1982) and reproduced here in Fig. 1.

Our simulations successfully reproduce this eddy. In all simulation results, the wavelet analysis tracks this eddy from its 'birth' (mid of July 2001 for 3-km simulations; end of June 2001 for 1-km simulations), to its 'death' (mid of August 2001). In fact, the simulation results show that, at the middle of August (the end of the eddy's life), the anticyclonic eddy approaches the Northern Current and interacts with it. Such interaction can be considered fatal to the eddy and brings its collapse. The eddy has a much stronger signal throughout his life compared to other modelled structures of the shelf. Nevertheless non negligible differences appear between simulations. These differences are due to both the model spatial resolution and the attenuation coefficient δ. Hence, in the following, we will present: i) the influence of the model spatial resolution and ii) of the attenuation coefficient, and iii) the validation of the best model configuration for eddies' simulation.

Firstly, we study the influence of the spatial resolution. Fig.2 shows that more small-scale processes are resolved, as expected, in the refined simulations. The intensity of the modelled relative vorticity in the 1-km simulations (*exp3* and *exp4*) is stronger than the one in the 3-km simulations (*exp0*, *exp1* and *exp2*). The site of the anticyclonic structure in the 1-km simulations is located more North than the site of the eddy in the 3-km simulations. Moreover (Table 1), the eddy in the 1-km simulations has a much longer tracking duration (56-70 days) than the eddy in the 3-km simulations (33-45 days). As we mentioned previously, since the 'death' of this eddy in each simulation is occurring at the same period, the differences in tracking duration are due to the differences in the starting date of the eddy. At the beginning of the eddy's life determined in the 1-km simulations, the eddy area is very small; hence the 3-km simulations can not reproduce it. Furthermore, the ring of cyclonic vorticity, indicating the outer edge of the anticyclonic circulation, is much better represented in the nested simulations than in the coarse model ones (Fig. 3b-f). We compared our numerical results with satellite data. Fig. 3a shows a chlorophyll *a* situation typical of the time period of interest. The eddy structure is identified by a relatively low chlorophyll *a* concentration (0.1 mg m^{-3}) contoured on its northern edge (43°15'N, 3°30'E) by a high chlorophyll *a* plume extending southeastward and indicating the clockwise rotation of the anticyclonic eddy. The large size and northern position of the eddy in the satellite imagery match the high-resolution model results better than the low-resolution model ones. However, the size differences between the simulations (Table 1) are not obvious to interpret because of the high temporal variability of the eddy. This effect is probably due not only to the horizontal resolution but also to the horizontal diffusion.

For this reason, secondly, we study the influence of the coefficient δ in the horizontal diffusion term. We observed that the variation of the δ coefficient does not change the general position of the eddy in the 3-km simulations or in the 1-km ones (Fig. 3). Nevertheless, with increasing attenuation coefficient δ, the diffusion effect becomes more important. As shown in Table 1, for each resolution, the mean eddy area increases as the structure becomes more diffusive when δ increases from 0.2 to 0.8. Furthermore, the influence of the variation of δ is more important in the coarse-resolution simulations than in the fine-resolution ones. Visual analysis of all simulations with $\delta = 0.8$ show that (sub) mesoscale structures tend to completely disappear in the 3-km resolution simulations but not completely in the 1-km resolution ones. Moreover, for the 3-km simulations, when δ goes from 0.2 to 0.8, the standard deviation of *exp2* increases dramatically (Table 1), indicating the lack of realism of the *exp2* results. Whereas, for the 1-km simulations, the influence of the change of δ on the standard deviation is not significant, meaning that the eddy size and position do not change much. Moreover, we observed that the result of *exp3* (δ=0.2) displays considerable small-scale noise, or, in other words, that the dissipative effect is too weak. At the same time a more realistic coherence of the eddy and a decrease in small-scale noise are gained with an increased diffusion (*exp4*). Indeed, the eddy structure in *exp3* (Fig. 3e) is more heterogeneous than the one in *exp4* (Fig. 3f). This heterogeneity separates the eddy into several substructures and complicates the wavelet identification. This heterogeneity, present in the modelled relative vorticity, does not have a counterpart in the satellite chlorophyll concentration (Fig. 3a).

Combining the effects of both the model resolution and the coefficient δ, and preliminary comparison of results to satellite observations, we can deduce that the best simulation to reproduce anticyclonic eddies in our study area has a 1-km resolution and an attenuation coefficient δ of 0.8 in the horizontal diffusion term, as in *exp4*.

Hence, thirdly, we are going to validate this chosen configuration. As explained before, we have compared the eddies' size in the results of simulation *exp4* and the satellite images. Despite the discontinuity in the satellite images due to cloud coverage, this anticyclonic structure has been observed very clearly 13 times during its lifetime, between the middle of July (July 11, 2005) and the middle of August (August15, 2001). The longest gap in the data - when we have no satellite observations - is 6 days. Before mid July, a small structure was also detected in the same area and period as the one reproduced by the 1-km simulations and detected by the wavelet analysis. Further study would be needed to verify its rotation direction and, if anticyclonic, whether it corresponds or not to the origin of our eddy as suggested by the nested model. We tried to estimate the area of the eddy from the thirteen satellite images available during its lifetime.We subjectively contoured the eddy by a circle, which area is then compared to the corresponding area obtained by

the wavelet analysis. The circle area of Fig. 3a is, for example, equal to 1950 km^2. It is in good agreement with the instantaneous value obtained from *exp4* (2103 km^2), knowing that this latter is slightly overestimated since a small 'tail' (high vorticity leaving the eddy on its south side) is included in the wavelet identification. In the satellite data, the minimum value is 1146 km^2 estimated on July 11, 2001, corresponding to the first satellite observation. The maximum value is 2223 km^2 estimated on July 30, 2001, corresponding to the half period of the satellite observations. In the last observation, the eddy area is 1962 km^2, and the averaged eddy area within the period of satellite observations is 1786 ± 384 km^2. These values fit nicely within the range 1193 ± 543 km^2 obtained with the *exp4* simulation (Table 1). Moreover, the agreement is even better when the values are compared to 1442 ± 598 km^2 obtained in averaging the corresponding thirteen *exp4* simulation. Despite the subjective character of this estimation, these values allow us to say that *exp4* is in good agreement with the observations.

4 Conclusions

In order to accurately simulate the (sub)mesoscale structures in the GoL, we have studied the impacts of the model resolution and of an attenuation coefficient in the advection-diffusion scheme. An anticyclonic eddy, in good agreement with satellite imagery as far as its size and position, is for the first time reproduced numerically, in the western side of the gulf of Lion, by choosing a model setup of 1-km spatial resolution and an attenuation coefficient of 0.8 for the horizontal diffusion. Its average area is about 1200 km^2 and it lasts about 60 days. It is also the first time that a wavelet technique is used to detect (sub)mesoscale structures in the coastal waters. As expected (Nof, 1999), the model and wavelet analysis results show that this anticyclonic eddy is nearly constant in its position during its life time. Future work will focus on the study of the generating processes and mechanisms of these anticyclonic eddies, and will try to identify its potential impact on shelf-offshore exchanges. Furthermore, the numerical modeling will help us set up the sampling strategy of the main LATEX cruise, which plans to focus on this eddy structure. The in situ measurements combined with the modeling results will allow us to well understand the eddies' dynamics.

Acknowledgements

The authors warmly thank Emmanuel Bosc for the satellite data. The MODIS Aqua data were supplied by the Distributed Active Archive Center at NASA

Goddard Space Flight Center and made possible by the MODIS Project. The LATEX projet is supported by the programs LEFE/IDAO and LEFE/CYBER of INSU-Institut National des Sciences de l'Univers and by the Region PACA-Provence Alpes Côte d'Azur. Z.Y. HU is financed by a MENRT Ph.D grant.

References

Albérola, C., Millot, C., 2003. Circulation in the french mediterranean coastal zone near marseilles: the influence of the wind and the northern current. Cont. Shelf Res 23, 587–610.

Auclair, F., Marsaleix, P., De Mey, P., 2003. Space-time structure and dynamics of the forecast error in a coastal circulation model of the Gulf of Lions. Dyn. Atmos. Oceans 36, 309–346.

Auclair, F., Marsaleix, P., Estournel, C., 2001. The penetration of the Northern Current over the Gulf of Lion (Mediterranean) as a downscaling problem. Oceanol. Acta 24, 529–544(16).

Bouffard, J., Vignudelli, S., Herrmann, M., Lyard, F., Marsaleix, P., Ménard, Y., Cipollini, P., 2008. Comparison of ocean dynamics with a regional circulation model and improved altimetry in the North-western Mediterranean. In: Terrestrial, Atmospheric and Oceanic Sciences. Vol. 19. pp. 117–133.

Conan, P., Millot, C., 1995. Variability of the Northern Current off Marseilles, western Mediterranean Sea, from February to June 1992. Oceanol. Acta 182, 193–205.

Doglioli, A. M., Blanke, B., Speich, S., Lapeyre, G., 2007. Tracking coherent structures in a regional ocean model with wavelet analysis: application to Cape Basin Eddies. J. Geophys. Res. 112.

Dufau-Julliand, C., Marsaleix, P., Petrenko, A., Dekeyser, I., 2004. Three-dimensional modeling of the Gulf of Lion's hydrodynamics (northwest Mediterranean) during January 1999 (MOOGLI3 Experiment) and late winter 1999: Western Mediterranean Intermediate Water's (WIW's) formation and its cascading over the shelf break. J. Geophys. Res. 109.

Estournel, C., 2001. The Rhone River Plume in Unsteady Conditions: Numerical and Experimental Results. Estuarine Coastal and Shelf Science 53, 25–38.

Estournel, C., Auclair, F., Lux, M., Nguyen, C., Marsaleix, P., 2007. "Scale oriented" embedded modeling of the North-Western Mediterranean in the frame of MFSTEP. Ocean Science Discussions 4, 145–187.

Estournel, C., Durrieu de Madron, X., Marsaleix, P., Auclair, F., Julliand, C., Vehil, R., 2003. Observation and modeling of the winter coastal oceanic circulation in the Gulf of Lions under wind conditions influenced by the continental orography (FETCH experiment). J. Geophys. Res. 108 (C3), 7–1,7–18.

Gaspar, P., Grégoris, Y., Lefevre, J.-M., 1990. A simple eddy kinetic energy

model for simulations of the oceanic vertical mixing: Tests at Station Papa and long-term upper ocean study site. J. Geophys. Res. 95, 179–193.
Gatti, J., 2008. Intrusions du Courant Nord Méditérranée sur la partie est du plateau continental du Golfe du Lion. Ph.D. thesis, Université de la Méditerranée.
Grilli, F., Pinardi, N., 1998. The computation of Rossby radii dynamical processes of deformation for the Mediterranean Sea. MTP News 6, 4.
Herrmann, M., Somot, S., Sevault, F., Estournel, C., Déqué, M., 2008. Modeling the deep convection in the northwestern Mediterranean Sea using an eddy-permitting and an eddy-resolving model: Case study of winter 1986-1987. J. Geophys. Res. 113.
Herrmann, M. J., Somot, S., 2008. Relevance of ERA40 dynamical downscaling for modeling deep convection in the Mediterranean Sea. Geophys. Res. Lett. 35.
James, I., 1996. Advection schemes for shelf sea models. J. Mar. Sys. 8, 237–254.
Jameson, L., Miyama, T., 2000. Wavelet analysis and ocean modeling: A dynamically adaptive numerical method "WOFD-AHO". Mon. Wea. Rev. 128, 1536–1548.
Luo, J., Jameson, L., 2002. A wavelet-based technique for identifying, labeling, and tracking of ocean eddies. J. Atmos. Ocean. Technol. 19 (3), 381–390.
Marsaleix, P., 1998. A numerical study of the formation of the Rhône River plume. J. Mar. Sys. 14, 99–115.
Marsaleix, P., Auclair, F., Estournel, C., 2006. Considerations on Open Boundary Conditions for Regional and Coastal Ocean Models. J. Atmos. Ocean. Technol. 23, 1604–1613.
Marsaleix, P., Auclair, F., Floor, J., Herrmann, M., Estournel, C., Pairaud, I., Ulses, C., 2008. Energy conservation issues in sigma-coordinate free-surface ocean models. Ocean Model. 20, 61–89.
Millot, C., 1979. Wind induced upwellings in the Gulf of Lions. Oceanol. Acta 2, 261–274.
Millot, C., 1982. Analysis of upwelling in the Gulf of Lions. In: Nihoul J. C. J. (Ed.), Hydrodynamics of semi-enclosed seas: Proceedings of the 13th International Liège Colloquium on Ocean Hydrodynamics. Elsevier Oceanogr. Ser. Vol. 34. Elsevier Sc. Pub, Amsterdam, The Netherlands, pp. 143–153.
Millot, C., 1990. The Gulf of Lions' hydrodynamics. Cont. Shelf Res. 10, 885–894.
Nof, D., 1999. Strange encounters of eddies with walls. J. Mar. Res. 57 (5), 739–761.
Petrenko, A. A., 2003. Variability of circulation features in the Gulf of Lion NW Mediterranean Sea. Importance of inertial currents. Oceanol. Acta 26, 323–338.
Petrenko, A. A., Dufau-Julliand, C., Estournel, C., 2008. Barotropic eastward currents in the western Gulf of Lion, northwestern Mediterranean Sea, dur-

359 ing stratified conditions. J. Mar. Sys. 74, 406–428.
360 Petrenko, A. A., Leredde, Y., Marsaleix, P., 2005. Circulation in a stratified
361 and wind-forced Gulf of Lions, NW Mediterranean Sea: in situ and modeling
362 data. Cont. Shelf Res. 25, 7–27.
363 Spall, M. A., Holland, W. R., 1991. A Nested Primitive Equation Model for
364 Oceanic Applications. J. Phys. Oceanogr. 21, 205–220.
365 Ulses, C., Estournel, C., Bonnin, J., Durrieu de Madron, X., Marsaleix, P.,
366 2008a. Impact of storms and dense water cascading on shelf-slope exchanges
367 in the Gulf of Lion (NW Mediterranean). J. Geophys. Res. 113.
368 Ulses, C., Estournel, C., Puig, P., Durrieu de Madron, X., Marsaleix, P., 2008b.
369 Dense shelf water cascading in the northwestern mediterranean during the
370 cold winter 2005: Quantification of the export through the gulf of lion and
371 the catalan margin. Geophys. Res. Lett. 35.
372 Ulses, C., Grenz, C., Marsaleix, P., Schaaff, E., Estournel, C., Meulé, S.,
373 Pinazo, C., 2005. Circulation in a semi enclosed bay under the influence
374 of strong fresh water input. J. Mar. Sys. 56, 113–132.

List of Figures

List of Tables

Contents